Laser and Particle Beams (2009), *27*, 79–84. Printed in the USA.
Copyright © 2009 Cambridge University Press 0263-0346/09 $20.00
doi:10.1017/S0263034609000111

Equations of State and the ellipsometry diagnostics

L. BAKSHI,[1,2] S. ELIEZER,[1] Z. HENIS,[1] N. NISSIM,[1] L. PERELMUTTER,[1] D. MORENO,[1] M. SUDAI,[1] AND M. MOND[2]

[1]Soreq NRC, Yavne 81800, Israel
[2]Mechanical Engineering, Ben Gurion University, Beer Sheva 84105, Israel

(RECEIVED 8 October 2008; ACCEPTED 19 November 2008)

Abstract

An overview of the equations of state (EOS) with a short summary of shock wave experiments with laser induced impact flyer, relevant to EOS study, is presented. The "old-new" ellipsometry is suggested and described for the EOS research. The detection of phase transitions of the first kind (solid-solid) as well as phase transition of the second kind (Curie point as an example) is demonstrated. Furthermore, the temperature measurements are not possible without the knowledge of the emissivity, a parameter that can be measured by using ellipsometry techniques.

Keywords: Ellipsometry diagnostics; Equation of state; Inertial confinement fusion

1. INTRODUCTION

The equation of state (EOS) describes a physical system by the relation between its thermodynamic quantities, such as pressure, energy, density, entropy, specific heat, etc., and is related to both fundamental physics and the applied sciences (Lomonosov, 2007; Tahir *et al.*, 2007*a*, 2007*b*, 2007c, 2008*a*, 2008*b*; Lebo *et al.*, 2008). Local thermodynamic equilibrium of nature can be described by a wide range of EOS pressure, density, and temperatures. For example, Figure 1 represents schematically various systems in the temperature-electron density domain. A route to inertial confinement fusion (ICF) leading to a solution of the energy problem is shown in this figure. As can be seen from this schematic figure, the well known low density ideal EOS gas as well as the extremely high density Thomas Fermi (TF) EOS cannot describe correctly the ICF problem, and therefore more complicated (i.e., realistic) EOS are needed. Since it is not yet known how to describe quantitatively the material at every available thermodynamic state, including all phases of the matter, it is necessary to introduce simplified methods whose range of applicability is limited. So far this is the attitude taken for EOS-ICF calculations (Eliezer *et al.*, 2007).

The EOS is derived from a thermodynamic potential. There are equivalent thermodynamic potentials related to each other by a Legendre transformation. The Legendre transformation between two potentials F and Ψ for several variables is defined by

$$\Psi(P_1, P_2, \ldots P_n) = F(X_1, X_2, \ldots X_n) - \sum_{i=1}^{n} P_i X_i; \quad P_i = \frac{dF}{dX_i}$$
$$d\Psi(P_1, P_2, \ldots P_n) = dF - \sum_{i=1}^{n} (P_i dX_i + dP_i X_i), \tag{1}$$

where the conjugate variable of X_i is P_i. For example, the conjugate variables of entropy and specific volume (S, V) are the temperature and pressure (T, P) accordingly. Assuming a system with a constant number of particles, $N =$ const., the Gibbs potential G is derived from the internal energy E by the following Legendre transformation

$$G(T, P) = E(S, V) - \left[\left(\frac{\partial E}{\partial S}\right)_V S + \left(\frac{\partial E}{\partial V}\right)_S V\right];$$
$$\Rightarrow G = E - TS + PV. \tag{2}$$

A summary of the thermodynamic potentials, derived from each other by a Legendre transformation is given in Table 1. The thermodynamic potentials are: $E =$ internal energy, $H =$ enthalpy, $F =$ Helmholtz' free energy, $\mathbf{G} =$ Gibbs' free energy, and $\Phi =$ the grand potential. The appropriate variables of the potentials are denoted by $V =$

Address correspondence and reprint requests to: Shalom Eliezer, Soreq NRC, Yavne 81800, Israel. E-mail: shalom.eliezer@gmail.com

https://doi.org/10.1017/S0263034609000111 Published online by Cambridge University Press

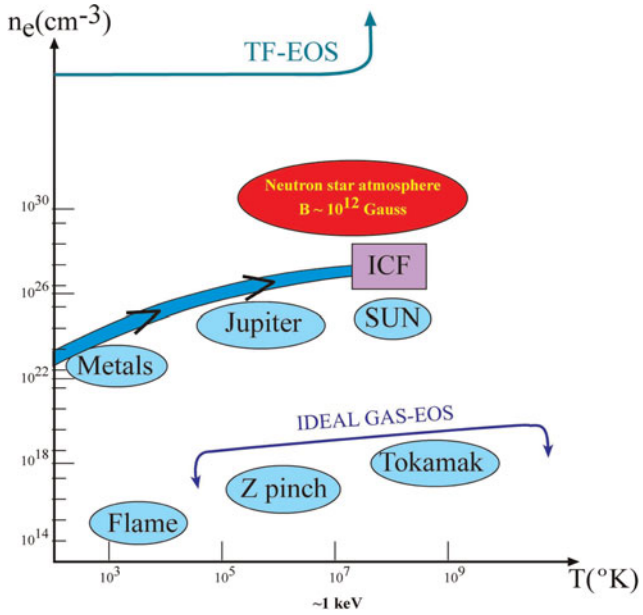


Fig. 1. (Color online) The route to inertial confinement fusion (ICF) in the electron density (n) –temperature (T) plane. The Z pinch and Tokamak plasmas are described by the ideal gas equation of state (EOS), the Thomas Fermi (TF) EOS describe matter at very high densities while the route to ICF is described by complicated EOS.

specific volume $= 1/\rho$ where ρ is the density, $T =$ temperature, $P =$ pressure, $S =$ entropy, $\mu =$ chemical potential, and $N =$ the number of particles. The various EOS derived from these potentials are summarized in Table 1. As one can see from this table, there are many possible presentations of EOS.

The starting points in analyzing the one-dimensional fluid equations described by the conservation laws of mass, momentum, and energy is given by,

$$\frac{\partial \rho}{\partial t} = -\frac{\partial}{\partial x}(\rho u), \tag{3}$$

$$\frac{\partial}{\partial t}(\rho u) = -\frac{\partial}{\partial x}(P + \rho u^2), \tag{4}$$

$$\frac{\partial}{\partial t}\left(\rho E + \frac{1}{2}\rho u^2\right) = -\frac{\partial}{\partial x}\left(\rho E u + P u + \frac{1}{2}\rho u^3\right). \tag{5}$$

The usual notation is used, where x-t is space-time, ρ is the density, u is the flow velocity, P is the pressure, and E is the internal energy per unit mass. These three equations have four unknowns: ρ-P-E-u and therefore another equation, namely the EOS is needed in order to solve the problem.

Table 1. *Equations of state for the various potentials: Specific energy* E*, Enthalpy* H*, Helmholtz Free Energy* F*, Gibbs potential* G *and the grand potential Φ. The thermodynamic variables for the potentials are given in the brackets of the first column, where the notation is: entropy* – S*, specific volume* – V*, pressure* – P*, temperature* – T*, μ is the chemical potential and the particle number is* N

Potential		Equations of State
$E(S, V, N)$	$dE = TdS - PdV + \mu dN$	$T = (\partial E/\partial S)_{V,N}$; $P = -(\partial E/\partial V)_{S,N}$; $\mu = (\partial E/\partial N)_{S,V}$;
$H(S, P, N)$	$dH = TdS + VdP + \mu dN$	$T = (\partial H/\partial S)_{P,N}$; $V = (\partial H/\partial P)_{S,N}$; $\mu = (\partial H/\partial N)_{S,P}$;
$F(T, V, N)$	$dF = -SdT - PdV + \mu dN$	$S = -(\partial F/\partial T)_{V,N}$; $P = -(\partial F/\partial V)_{T,N}$; $\mu = (\partial F/\partial N)_{T,V}$;
$G(T, P, N)$	$dG = -SdT + VdP + \mu dN$	$S = -(\partial G/\partial T)_{P,N}$; $V = (\partial G/\partial P)_{T,N}$; $\mu = (\partial G/\partial N)_{T,P}$;
$\Phi(T, V, \mu)$	$d\Phi = = - SdT - PdV - Nd\mu$	$S = -(\partial \Phi/\partial T)_{V,\mu}$; $P = -(\partial \Phi/\partial V)_{T,\mu}$ $N = -(\partial \Phi/\partial \mu)_{T,V}$;

2. SHOCK WAVES

The science of EOS (Eliezer *et al.*, 1986; Eliezer & Ricci, 1991; Bushman *et al.*, 1993; Batani *et al.*, 1999, 2007; Desai *et al.*, 2007; Lomonosov, 2007; Eliezer & Henis, 2008) is studied experimentally in the laboratory by using static and dynamic techniques. In static experiments, the sample is squeezed between pistons or anvils. The conditions in these static experiments are limited by the strength of the construction materials. In the dynamic experiments, shock waves are created (Zeldovich & Raizer, 1966). Since the passage time of the shock is short in comparison with the disassembly time of the shocked sample, one can do shock wave research for any pressure that can be supplied by a driver, assuming that a proper diagnostic is available. In the scientific literature, the following shock-wave generators are discussed: a variety of guns (such as rail guns and two stage light-gas gun) that accelerate a foil to collide with a target, exploding foils, magnetic compression, chemical explosives, nuclear explosions, and high power lasers (Eliezer, 2002; Evans *et al.*, 1996; Batani *et al.*, 1996; Rothman *et al.*, 2002; Koening *et al.*, 2004). Conventional high explosives and gun drivers can achieve pressures up to a few mega-bars, while with the high power lasers; up to one giga-bar pressure has been achieved. The Nova laser from Livermore laboratories created a pressure of 750 $\pm$ 200 Mbar (Cauble *et al.*, 1993). This was achieved in a collision between two gold foils, where the flyer (Au foil) was accelerated by a high intensity X-ray flux created by the laser plasma interaction.

If the initial flow velocity is $u_0 \neq 0$, then the conservation laws (mass, momentum, and energy) in the laboratory frame of reference can be written

$$\textbf{lab.frame}\begin{cases} \rho_0(u_s - u_0) = \rho_1(u_s - u_p) \\ \rho_0(u_s - u_0)(u_p - u_0) = P_1 - P_0 \\ \rho_0(u_s - u_0)\left(E_1 - E_0 + \frac{1}{2}u_p^2 - \frac{1}{2}u_0^2\right) \\ = P_1 u_p - P_0 u_0 \end{cases}.$$

https://doi.org/10.1017/S0263034609000111 Published online by Cambridge University Press

These equations are called the Hugoniot relations. These relations are used to determine the state of the compressed solid behind the shock front. Assuming that the initial state is well defined and the quantities E_0, u_0, P_0, and ρ_0 are known, one has FIVE unknowns E_1, u_p, P_1, ρ_1, and u_s with three equations. Usually the shock wave velocity is measured experimentally, and if the EOS is known (in this case, one has four equations) $E = E(P, \rho)$ then the quantities of the compressed state can be calculated. If the EOS is not known, then one has to measure experimentally two quantities of the shocked material, for example, u_s and u_p, in order to solve the problem.

It was found experimentally (McQueen, 1991) that for many solid materials, initially at rest ($u_0 = 0$), the following linear relation between the shock velocity u_s and the particle velocity u_p is valid to a very good approximation

$$u_s = c_0 + \alpha u_p, \tag{6}$$

where c_0 and α are constants. c_0 is the bulk sound speed at standard conditions, where c_0 is related to the longitudinal (c_L), and transversal (c_t) velocities of the sound,

$$c_0 = \sqrt{c_L^2 - \frac{4}{3}c_t^2}. \tag{7}$$

Eq. (6) is an EOS along the Hugoniot line by taking into account the Hugoniot relations, where the shock and particle velocities are expressed by the appropriate density and pressure.

The laser driven matter under extreme conditions for EOS studies is achieved by: (1) laser produced shock waves in direct drive, (2) X-ray produced shock waves in hohlraum drive, and (3) shock wave by impact with laser (direct or indirect) launched flyer plate. For accurate EOS measurements, a uniform shock wave is required, steady state pressure, and no preheating. For example, 1% accuracy in velocity measurements for $\sim$1 mm target size and $\sim$1 ns measurement time, it is necessary to have 10 μm spatial resolutions and 10 ps temporal resolutions.

3. IMPACT BY AN ACCELERATING FOIL

The highest laser induced pressures, $\sim 10^8$–10^9 atmospheres have been obtained during the collision of a target with an accelerating foil. This acceleration was achieved by laser-produced plasma, or by X-rays from a cavity produced by laser plasma interactions. It is therefore now shown how the pressure is calculated in a planar collision between a flyer and a target.

The flyer has a known (i.e., measured experimentally) initial velocity before impact, u_f. The initial state before collision is for the target (B) $u_p = 0$ and $P = 0$, while for the flyer (A) $u_p = u_f$, and $P = 0$. Upon impact, a shock wave moves forward into B, and another shock wave goes into the flyer in the opposite direction. The pressure and the particle velocity are continuous at the interface of target and flyer. Therefore, the particle velocity of the target changes from zero to u, while the particle velocity in the flyer changes from u_f to u. Moreover, the pressure in the flyer plate A equals the pressure in the target plate B, and if the EOS are known and given by the linear $u_s - \underline{u}_p$ relation and the second Hugoniot equation is used to calculate the pressure, one gets

$$P_H = \rho_{0B} u(c_{0B} + \alpha_B u) = \rho_{0A}(u_f - u)[c_{0A} + \alpha_A(u_f - u)]. \tag{8}$$

This is a quadratic equation in u, with the following solution

$$\begin{aligned} u &= \frac{-b - \sqrt{b^2 - 4ac}}{2a} \\ a &\equiv \rho_{0A}\alpha_A - \rho_{0B}\alpha_B; \\ b &\equiv -(c_{0A}\rho_{0A} + c_{0B}\rho_{0B} + 2\rho_{0A}\alpha_A u_f) \\ c &\equiv (c_{0A}\rho_{0A} + \rho_{0A}\alpha_A u_f)u_f. \end{aligned} \tag{9}$$

Once the flow velocity u is known, it is substituted in the above equation to derive the pressure. If the EOS of the target is not known, then it is necessary to measure the shock wave velocity u_{sB}. In this case, the pressure equality in the flyer and the target yields

$$P_H = \rho_{0B} u_{sB} u = \rho_{0A}[c_{0A} + \alpha_A(u_f - u)](u_f - u). \tag{10}$$

Note that in this equation, u_{sB} is known. The solution of this equation is

$$u = u_f + w - \left[w^2 + \left(\frac{\rho_{0B}}{\rho_{0A}\alpha_A}\right)u_{sB}u_f\right]^{1/2} \tag{11}$$

$$w \equiv \frac{1}{2\alpha_A}\left(c_{0A} + \frac{\rho_{0B}u_{sB}}{\rho_{0A}}\right). \tag{12}$$

In these types of experiments, it is occasionally convenient to measure the free surface velocity of the target in order to calculate the particle velocity.

Foils are used to impact stationary targets and reach pressures of hundreds of Mega-bar. In this method, the flyer stores kinetic energy from the driver, which may be a laser or X-rays, and delivers it much rapidly as thermal energy during collisions. In addition, the flyer serves as a preheat shield so that the target remains on a lower adiabat. The flyer technique was demonstrated using a laser as driver (Obenschain *et al.*, 1983) and later applied to achieve pressures of more than 100 Mbar (Fabbro *et al.*, 1986). At ILE, Osaka University in Japan (H. Azechi, 2008, private communication), the highest pressure was achieved, 410 ± 60 Mbar, with a direct drive laser induced flyer. The flyer, a plastic foil of 14 μm thickness doped with 0.3% CHBr (for Rayleigh Taylor stability), was accelerated to a final

https://doi.org/10.1017/S0263034609000111 Published online by Cambridge University Press

velocity of 640 km/s, and during its collision with a copper target, the pressure of ~400 Mbar was achieved. At Livermore, the flyer technique was used (plastic-gold flyer on a gold target) with X-ray created by Nova to produce over ~700 Mbar in a planar shock (Cauble *et al.*, 1993), enabling first experimental measurements of EOS in the giga-bar regime.

4. THE ELLIPSOMETRY PROPOSAL FOR LASER-PLASMA INTERACTIONS

Ellipsometry measures the polarization-dependent reflectivity of a probe beam from a surface and can distinguish the real and imaginary parts of the time dependent complex index of refraction $N(\omega) = n + ik$, giving access to fundamental properties of the material, such as phase transitions (Nissim *et al.*, 2007) and electrical conductivity. ω is the probe laser frequency.

The polarization state of the light, incident upon the sample, may be decomposed into an *S* and a *P* component (the *S* component is oscillating perpendicular to the plane of incidence and parallel to the sample surface, and the *P* component is oscillating parallel to the plane of incidence, see Fig. 2). The amplitudes of the *S* and *P* components, after reflection and normalized to their initial value, are denoted by r_s and r_p, respectively. Ellipsometry measures the ratio η of r_s and r_p. The absolute value of the reflected amplitudes ratio (denoted by $\tan\psi$) and the phase difference Δ are determined by six photo-multiplier detectors as described in Figure 3 for the general case where polarization is not necessarily 100%. Previously, Yoneda *et al.* (2003) suggested a scheme with four photo-multipliers where one requires 100% polarization. In our impact experiments with gas gun or even in high pressure static experiments, it was found that polarization can be reduced occasionally to 10%.

In Figure 3, the experimental setup for the ellipsometry measurement is described with six photo-multipliers (PMT). The incident diagnostic laser passes through a polarizer with an intensity I_{tot} before hitting the target under consideration. The scattered laser is deflected by a beam splitter *via* a quarter wave plate to derive circular polarizations, right and left with intensities I_{rcp} and I_{lcp} accordingly, into PMT 5 and 6 that measure intensities I_5 and I_6. The laser that passes the first beam splitter is deflected by a second beam splitter *via* a half wave plate to obtain linear polarizations at +45 and −45 degrees with intensities I_{+45} and I_{-45} accordingly into PMT 3 and 4 that measure intensities I_3 and I_4. Finally, the PMT 1 and 2 measure I_1 and I_2 that corresponds to the *S* and *P* polarizations with intensities I_s and I_p accordingly. From the six PMT measurements, the Stokes vectors time dependent (s_0, s_1, s_2, s_3) are calculated according to the following relations

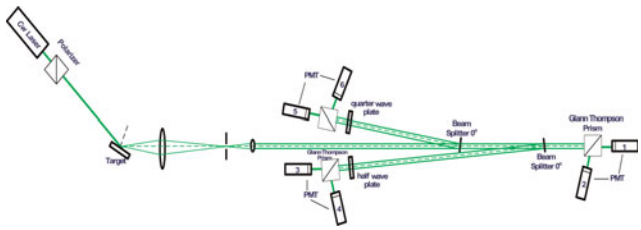


Fig. 3. (Color online) The experimental set up for the ellipsometry measurements. PMT from 1 to 6 are photo multipliers. The incident diagnostic laser passes through a polarizer before hitting the target under consideration. The scattered laser is deflected by a beam splitter via a quarter wave plate to derive circular polarizations (left and right) into PMT 5 and 6. The laser that passes the first beam splitter is deflected by a second beam splitter *via* a half wave plate to obtain linear polarizations (at +45 and −45 degrees) into PMT 3 and 4. Finally, the PMT 1 and 2 measure the *s* and *p* polarizations. From the six PMT measurements the Stokes vector (four parameters) are calculated.

$$\begin{pmatrix} s_0 \\ s_1 \\ s_2 \\ s_3 \end{pmatrix} \equiv \begin{pmatrix} I_{tot} \\ I_s - I_p \\ I_{=45} - I_{-45} \\ I_{rcp} - I_{lcp} \end{pmatrix} = \begin{pmatrix} 1 \\ (I_1 - I_2)/(I_1 + I_2) \\ (I_3 - I_4)/(I_3 + I_4) \\ (I_5 - I_6)/(I_5 + I_6) \end{pmatrix} \quad (13)$$

From the Stokes vector, the ratio η of the *P* to *S* polarization amplitudes is calculated for +45 degrees linear polarization laser probe beam (incident on target). Assuming that the refraction index N_0 is known, the degree of polarization, deg *P*, the complex index of refraction, N_1, and emissivity, ϵ, of the target (see Fig. 2) are derived.

$$\eta = \frac{r_p}{r_s} = \tan\psi e^{i\Delta}. \quad (14)$$

$$N_1 = N_0 \tan\varphi_0 \left[1 - \frac{4\eta}{(1+\eta)^2}\sin^2\varphi_0\right]^{1/2}. \quad (15)$$

$$\psi = \frac{1}{2}\tan^{-1}\left(\frac{\sqrt{s_2^2 + s_3^2}}{-s_1}\right); \Delta = \tan^{-1}\left(\frac{-s_3}{s_2}\right). \quad (16)$$

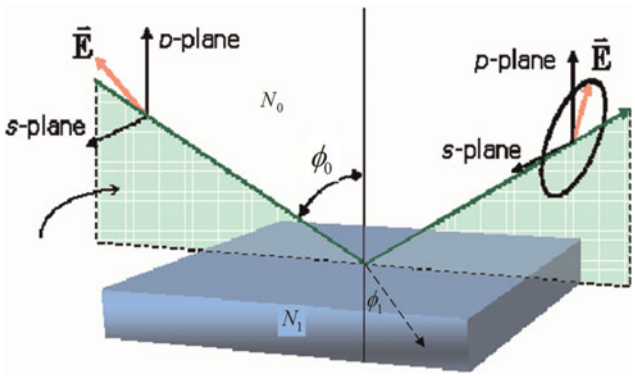


Fig. 2. (Color online) The ellipsometry scheme. N_0 and N_1 are the complex indices of refraction, ϕ_0 and ϕ_1 are the incident and the reflected angle, *E* is the laser electric field, and *s* and *p* are the two distinct polarizations.

https://doi.org/10.1017/S0263034609000111 Published online by Cambridge University Press

$$\deg P = \frac{(s_1^2 + s_2^2 + s_3^2)^{1/2}}{s_0}. \quad (17)$$

$$\varepsilon = 1 - \left|\frac{1-N}{1+N}\right|^2. \quad (18)$$

In laser induced shock waves studies, the ellipsometry is combined with other diagnostics, such as that using the velocity interferometer system for any reflector (VISAR), pyrometry or X-ray diffraction, providing a precise characterization of the dynamic properties of the material.

In order to show the power of ellipsometry in detecting phase transitions of the first kind (solid-solid and solid-liquid) and phase transitions of the second kind (the Curie transition), we present three very recent experiments using a 532 nm probe laser. The pressures where obtained with gas gun impact (Fig. 4), and temperatures experiments with pulsed power heating (Figs 5 and 6). In Figure 4, the emissivity change is shown during a solid-solid ($\alpha \rightarrow \varepsilon$) phase transition of 1020 steel (the upper line after the shock wave transition at 1.8 μs) in comparison with the change without a phase transition (the lower line). In Figure 5, the refractive index of nickel as a function of temperature is given where the upper line is imaginary part and the lower line the real index of refraction. Figure 6 describes the emissivity change of nickel during a phase transition of the second kind where a distinct change in the slope occurs near the Curie point. It is important to emphasize that in these experiments, all Stokes components were measured as described in Figure 3 and the above formulas.

We conclude this paper with the summary given in Figure 7, where the schematic flow chart shows the connection between the complex index of refraction and the EOS. The emissivity is required in order to obtain the temperature, one of the most important thermodynamic quantities

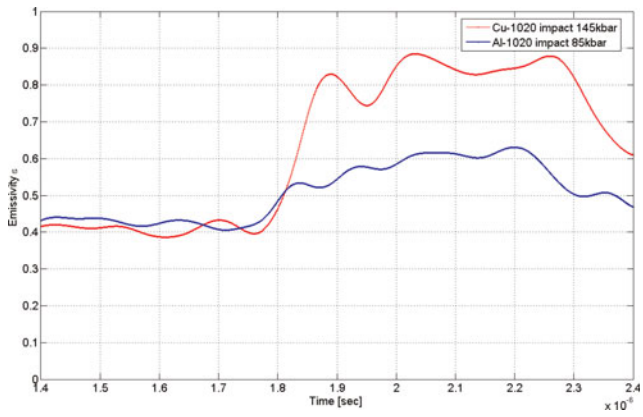


Fig. 4. (Color online) The emissivity change during a solid-solid ($\alpha \rightarrow \varepsilon$) phase transition of 1020 steel (the upper line after the shock wave transition at 1.8 μs) in comparison with the change without a phase transition (the lower line).

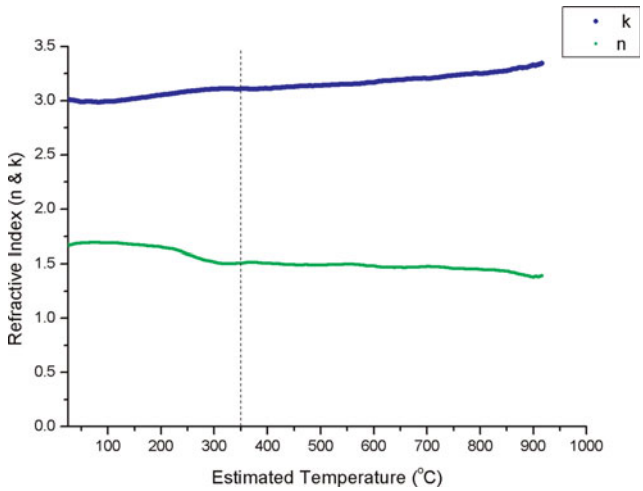


Fig. 5. (Color online) The complex refractive index of nickel as a function of temperature. The upper line is the complex index of refraction while the lower line is the real index of refraction.

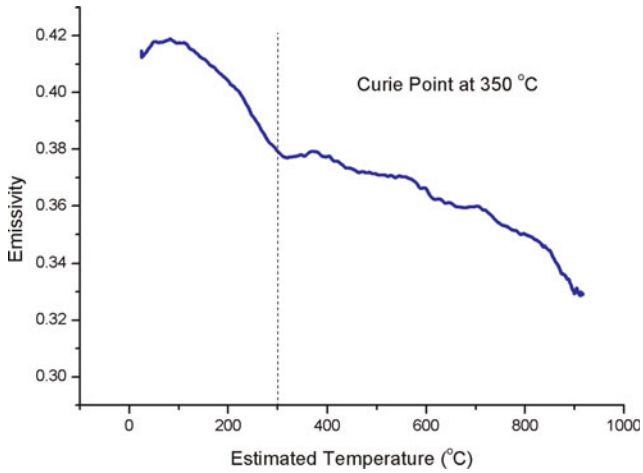


Fig. 6. (Color online) The emissivity change of nickel during a phase transition of second kind. The Curie point there is a distinct change in the slope.

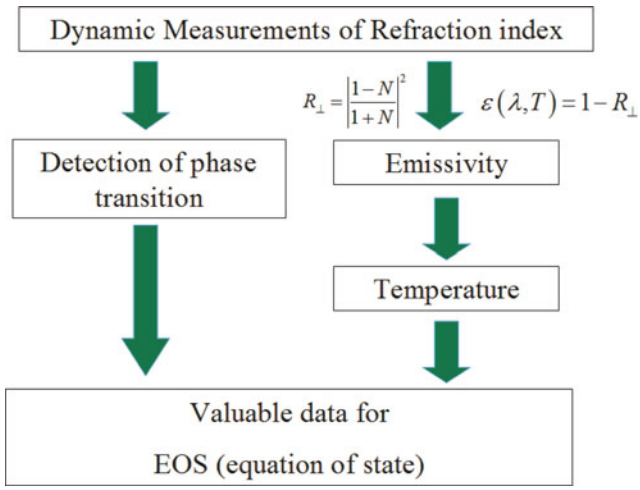


Fig. 7. (Color online) A schematic flow chart that shows the connection between the complex index of refraction and the equations of state.

https://doi.org/10.1017/S0263034609000111 Published online by Cambridge University Press

describing the EOS. The detection of the phase transition domains is an integral part of EOS.

REFERENCES

Batani, D., Bossi, S., Benuzzi, A., Koenig, M., Faral, B., Boudenne, J.M., Grandjouan, N., Atzeni, S. & Temporal, M. (1996). Optical smoothing for shock-wave generation: Applications to the measurement of equations of state. *Laser Part. Beams* **14**, 211–223.

Batani, D., Dezulian, R., Redaelli, R., Benocci, R., Stabile, H., Canova, F., Desai, T., Lucchini, G., Krousky, E., Masek, K., Pfeifer, M., Skala, J., Dudzak, R., Rus, B., Ullschmied, J., Malka, V., Faure, J., Koenig, M., Limpouch, J., Nazarov, W., Pepler, D., Nagai, K., Norimatsu, T. & Nishimura, H. (2007). Recent experiments on the hydrodynamics of laser-produced plasmas conducted at the PALS laboratory. *Laser Part. Beams* **25**, 127–141.

Batani, D., Keonig, M., Benuzzi, A., Krasyuk, I.K., Pashinin, P.P., Semenov, A.Yu., Lomonosov, I.V. & Fortov, V.E. (1999). Problems of measurement of dense plasma heating in laser shock wave compression. *Laser Part. Beams* **17**, 265–273.

Bushman, A.V., Kanel, G.I., Ni, A.L. & Fortov, V.E. (1993). *Intense Dynamic Loading of Condensed Matter*. Washington DC: Taylor and Francis.

Cauble, R., Phillion, D.W., Hoover, T.J., Holmes, N.C., Kilkenny, J.D. & Lee, R.W. (1993). Demonstration of 0.75 Gbar planar shocks in X-ray driven colliding foils. *Phys. Rev. Lett.* **70**, 2102–2105.

Desai, T., Dezulian, R. & Batani, D. (2007). Radiation effects on shock propagation in Al target relevant to equation of state measurements. *Laser Part. Beams* **25**, 23–30.

Eliezer, S. & Henis, Z. (2008). *Applications of Laser-Plasma Interactions*, chapter 6, (Eliezer S. & Mima K. eds.). Boca Raton: CRC Press.

Eliezer, S. & Ricci, R.A. (1991). *High Pressure Equations of State: Theory and Applications*. Amsterdam: North Holland Publishing.

Eliezer, S. (2002). *The Interaction of High-Power Lasers with Plasmas*. Bristol: Institute of Physics Publishing.

Eliezer, S., Ghatak, A. & Hora, H. (1986). *An Introduction to Equations of State: Theory and Applications*. Cambridge: Cambridge University Press.

Eliezer, S., Murakami, M. & Martinez-Val, J.M. (2007). Equation of state and optimum compression in inertial fusion energy. *Laser Part. Beams* **25**, 585–592.

Evans, A.M., Freeman, N.J., Graham, P., Horsfield, C.J., Rothman, S.D., Thomas, B.R. & Tyrrell, A.J. (1996). Hugoniot EOS measurements at Mbar pressures. *Laser Part. Beams* **14**, 113–123.

Fabbro, R., Faral, B., Virmont, J., Pepin, H., Cottet, F. & Romain, J.P. (1986). Experimental evidence of the generation of multi-hundred megabar pressures in 0.26 micron wavelength laser experiments. *Laser Part. Beams* **4**, 413–419.

Koenig, M., Henry, E., Huser, G., Benuzzi-Mounaix, A., Faral, B., Martinolli, E., Lepape, S., Vinci, T., Batani, D., Tomasini, M., Dasilva, L., Caubles, R., Hicks, D., Bradley, D., Mackinnon, A., Patel, P., Eggerts, J., Pasley, J., Willi, O., Neely, D., Notley, M., Danson, C., Borghesi, M., Romagnanis, L., Boehly, T. & Lee, K. (2004). High pressure generated by laser driven shocks: applications to planetary physics. *Nucl. Fusion* **44**, S208–S214.

Lebo, I.G., Lebo, A.I., Batani, D., Dezulian, R., Benocci, R., Jafer, R. & Krousky, E. (2008). Simulations of shock generation and propagation in laser-plasmas. *Laser Part. Beams* **26**, 179–188.

Lomonosov, I.V. (2007). Multi-phase equation of state for aluminum. *Laser Part. Beams* **25**, 567–584.

McQueen, R.G. (1991). *High Pressure Equations of State: Theory and Applications*. (Eliezer S. & Ricci R.A., eds.). Amsterdam: North Holland Publishing.

Nissim, N., Eliezer, S., Bakshi, L., Perelmutter, L., Moreno, D., Kot, E., Rozenberg, G.K.H. & Pasternak, M.P. (2007). High-pressure phase transition detection in diamond anvil cell using the method of ellipsometry. *J. Appl. Phys.* **102**, 106104–1/3.

Obenschain, S.P., Whitlock, R.R., Lean, E.A. & Ripin, B.H. (1983). Uniform ablative acceleration of targets by laser irradiation at 10^{14} W/cm^2. *Phys. Rev. Lett.* **50**, 44–48.

Rothman, S.D., Evans, A.M., Horsfield, C.J., Graham, P. & Thomas, B.R. (2002). Impedance match equation of state experiments using indirectly laser-driven multimegabar shocks. *Phys. Plasmas* **9**, 1721–1733.

Tahir, N.A., Kim, V., Lomonosov, I.V., Grigoriev, D.A., Piriz, A.R., Weick, H., Geissel, H. & Hoffmann, D.H.H. (2007*a*). High energy density physics problems related to liquid jet lithium target for Super-FRS fast extraction scheme. *Laser Part. Beams* **25**, 295–304.

Tahir, N.A., Kim, V., Matvechev, A., Ostrik, A., Lomonosov, I.V., Piriz, A.R., Lopez Cela, J.J. & Hoffmann, D.H.H. (2007*b*). Numerical modeling of heavy ion induced stress waves in solid targets. *Laser Part. Beams* **25**, 523–540.

Tahir, N.A., Kim, V.V., Matveichev, A., Ostrik, A., Shutov, A., Lomonosov, I.V., Piriz, A.R., Lopez Cela, J.J. & Hoffmann, D.H.H. (2008*a*). High energy density and beam induced stress related issues in solid graphite Super-FRS fast extraction targets. *Laser Part. Beams* **26**, 273–286.

Tahir, N.A., Schmidt, R., Brugger, M., Lomonosov, I.V., Shutov, A., Piriz, A.R., Udrea, S., Hoffmann, D.H.H. & Deutsch, C. (2007*c*). Prospects of high energy, density physics research using the CERN super proton synchrotron (SPS). *Laser Part. Beams* **25**, 639–647.

Tahir, N.A., Weick, H., Shutov, A., Kim, V., Matveichev, A., Ostrik, A., Sultanov, V., Lomonosov, I.V., Piriz, A.R., Cela, J.J.L. & Hoffmann, D.H.H. (2008*b*). Simulations of a solid graphite target for high intensity fast extracted uranium beams for the Super-FRS. *Laser Part. Beams* **26**, 411–423.

Yoneda, H., Morikami, H., Ueda, K. & More, R.M. (2003). Ultrashort pulse laser ellipsometric pump-probe experiments on gold targets. *Phys. Rev. Lett.* **91**, 0750041–4.

Zeldovich, Ya.B. & Raizer, Yu.P. (1966). *Physics of Shock Waves and High-Temperature Hydrodynamic Phenomena*. New York: Academic Press.

https://doi.org/10.1017/S0263034609000111 Published online by Cambridge University Press